

## Electronic Supplementary Information for

### Effects of Ga doping and hollow structure on the band-structures and photovoltaic properties of SnO<sub>2</sub> photoanode dye-sensitized solar cells

Yandong Duan,<sup>‡ab</sup> Jiaxin Zheng,<sup>‡a</sup> Nianqing Fu,<sup>bc</sup> Jiangtao Hu,<sup>a</sup> Tongchao Liu,<sup>a</sup> Yanyan Fang,<sup>b</sup> Qian Zhang,<sup>a</sup> Xiaowen Zhou,<sup>b</sup> Yuan Lin<sup>\*ab</sup> and Feng Pan<sup>\*a</sup>

<sup>a</sup>School of Advanced Materials, Peking University Shenzhen Graduate School, Shenzhen 518055, China

<sup>b</sup>Beijing National Laboratory for Molecular Sciences, Key Laboratory of Photochemistry, Institute of Chemistry, Chinese Academy of Sciences, Beijing 100190, China

<sup>c</sup>Department of Applied Physics, The Hong Kong Polytechnic University, Hung Hom, Kowloon, Hong Kong, China

<sup>d</sup>State Key Laboratory for Advanced Metals and Materials, School of Materials Science and Engineering, University of Science and Technology Beijing, Beijing 100083, China

‡These authors contributed equally to this work.

---

\*Corresponding author: [linyuan@iccas.ac.cn](mailto:linyuan@iccas.ac.cn) Tel: 86-10-82615031 Fax: 86-10-82617315

\*Corresponding author: [panfeng@pkusz.edu.cn](mailto:panfeng@pkusz.edu.cn) Tel: 86-755-26033200

The Fermi level of the photoanode in a DSSC is an important parameter because the difference between the red-ox potential in the quasi-Fermi level of the anode and the electrolyte determines the  $V_{oc}$  of the DSSCs. Flat band potentials ( $E_{fb}$ ) can be obtained from the intercept on the potential axis of Mott-Schottky plots using the equation

$$\frac{1}{C^2} = \left( \frac{2}{A^2 e \varepsilon \varepsilon_0 N_D} \right) (E - E_{fb} - \frac{kT}{e}),$$

where  $k$  the Boltzmann constant,  $T$  the absolute temperature,  $\varepsilon$  the dielectric constant of the  $\text{SnO}_2$  layer,  $\varepsilon_0$  the vacuum permittivity,  $e$  the electron charge,  $C$  represents the capacitance of the space charge region,  $N_D$  the donor density,  $E$  the applied potential,  $E_{fb}$  the flat band potential, and  $A$  is the active surface. As shown in Figure S1, the Mott-Schottky plots for the  $\text{SnO}_2$ ,  $\text{Sn}_{0.99}\text{Ga}_{0.01}\text{O}_2$ ,  $\text{Sn}_{0.97}\text{Ga}_{0.03}\text{O}_2$ ,  $\text{Sn}_{0.95}\text{Ga}_{0.05}\text{O}_2$  films at 1000Hz in the dark provided values of  $E_{fb}$  of 0.095, 0.016, -0.133, and -0.290 V (vs. SCE).

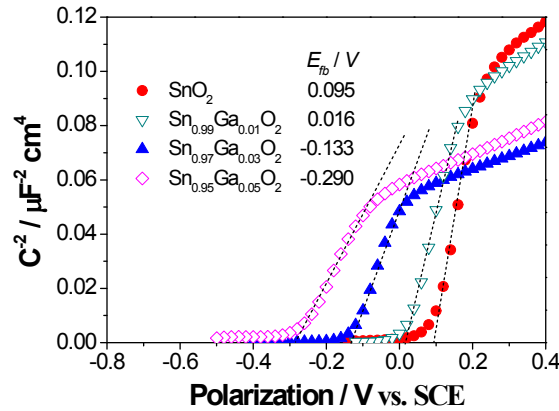


**Fig. S1.** Mott-Schottky plots of the  $\text{SnO}_2$  and the Ga-doped  $\text{SnO}_2$  films prepared on FTO substrates.

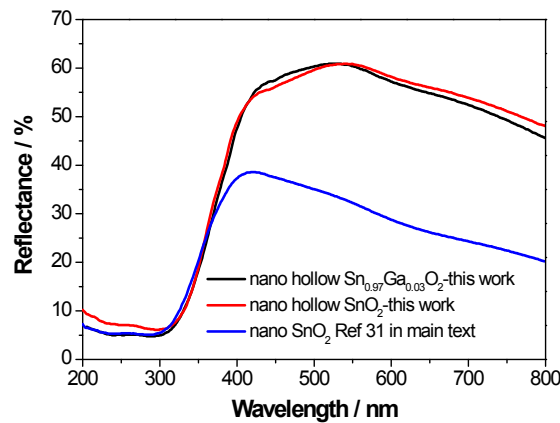


**Fig. S2.** Diffuse reflectance spectra of the photoelectrodes with nano  $\text{SnO}_2$ , nano hollow  $\text{SnO}_2$  and nano hollow  $\text{Sn}_{0.97}\text{Ga}_{0.03}\text{O}_2$ . The reflectance of the  $\text{SnO}_2$  and  $\text{Sn}_{0.97}\text{Ga}_{0.03}\text{O}_2$  hollow sphere films are much higher than that of the  $\text{SnO}_2$  nanocrystalline films, indicating that the particles in the hollow sphere film have a higher light scattering ability than those in the  $\text{SnO}_2$  nanocrystalline film.

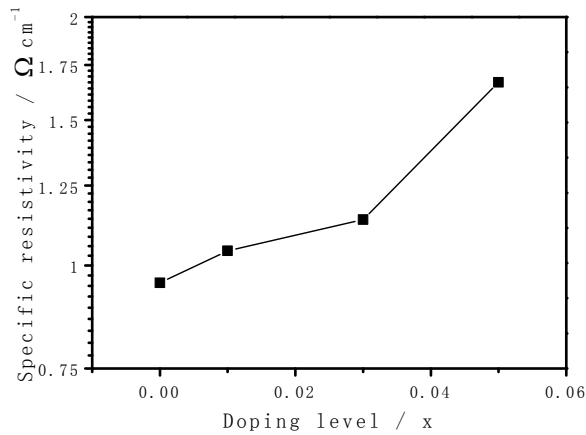


**Fig. S3.** Specific resistivity as a function of doping level for  $\text{Sn}_{1-x}\text{Ga}_x\text{O}_2$  films.

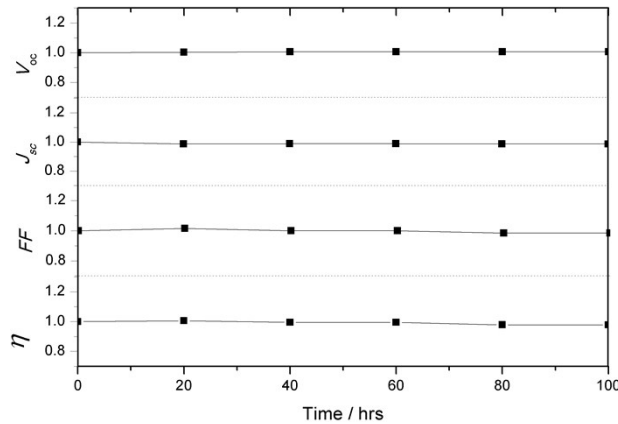


**Fig. S4.** Normalized device performance under constant illumination for 100h measured in air (DSSCs based on  $\text{Sn}_{0.97}\text{Ga}_{0.03}\text{O}_2/\text{TiCl}_4$ ). The values plotted in **Fig. S4.** are the averages over five samples. After 100 hrs, the conversion efficiency of DSSC is maintained at about 100% to the initial one.

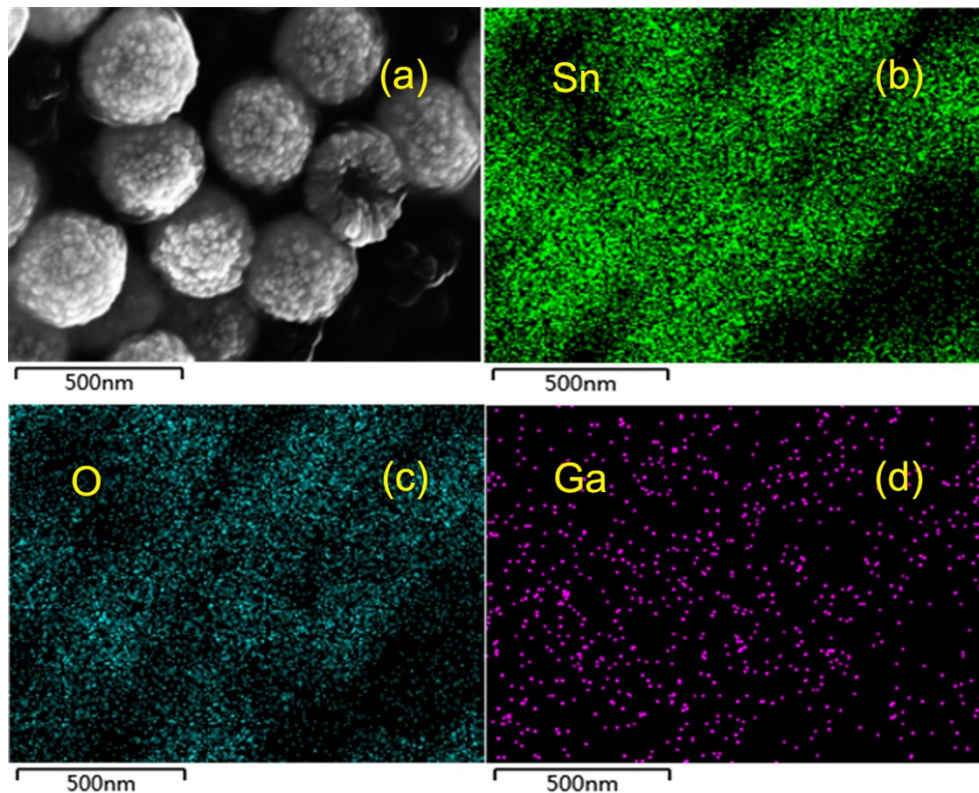


**Fig. S5.** (a) SEM image of the  $\text{Sn}_{0.97}\text{Ga}_{0.03}\text{O}_2$  synthesized from chemicals. (b)-(d) Elemental mapping performed from the SEM image (a). The elements (Sn, O, Ga) are uniformly distributed in the sample, indicative of the high homogeneity of the  $\text{Sn}_{0.97}\text{Ga}_{0.03}\text{O}_2$  particles.

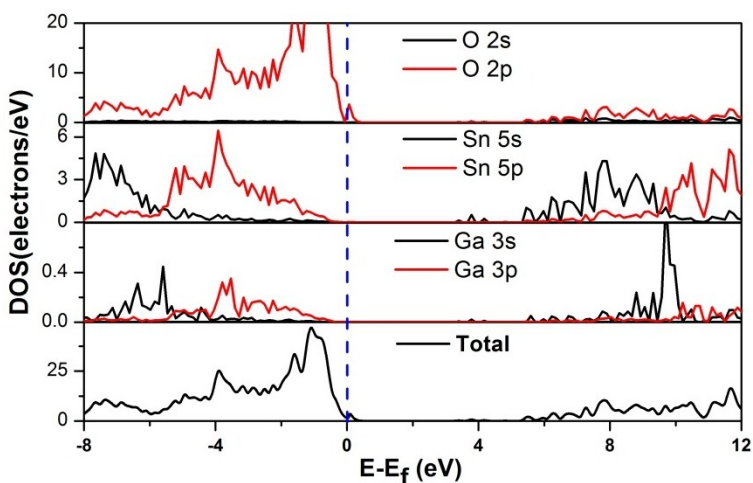


**Figure S6.** Calculated total and orbital resolved densities of states for the pure  $\text{SnO}_2$  and 6.25% Ga doped  $\text{SnO}_2$ . The Fermi level is set to zero.

**Table S1** The reported high values of  $\eta$  obtained in the DSSCs based on different SnO<sub>2</sub> photoanode structures.

| Ref.            | Morphology or structure                      | Diameter              | Synthetic method or manufacturer | Film thickness                    | $\eta$ (%) (no surface treatment) | $\eta$ (%) (after surface treatment) <sup>a</sup> |
|-----------------|--|-----------------------|----------------------------------|-----------------------------------|-----------------------------------|---|
| 1               | SnO <sub>2</sub> nanoparticles               | 3-5 nm                | Alfa Aesar                       | 10 $\mu\text{m}$                  | 1.74                              | MgO/7.21  |
| 2               | SnO <sub>2</sub> nanowire                    | 20-200nm              | reactive vapor transport         | 25-30 $\mu\text{m}$               | 2.1                               | TiCl <sub>4</sub> /4.1                            |
| 3               | SnO <sub>2</sub> hollow microspheres         | 1-2 $\mu\text{m}$     | hydrothermal                     | 10 $\mu\text{m}$                  | 1.4                               | TiCl <sub>4</sub> /5.65                           |
| 4               | SnO <sub>2</sub> nanoflower                  | 1 $\mu\text{m}$       | hydrothermal                     | 8-10 $\mu\text{m}$                | 3.00                              | TiCl <sub>4</sub> /6.78                           |
| 5               | SnO <sub>2</sub> nanoparticles               | 15 nm                 | Alfa Aesar                       | ---                               | 1.7                               | CaCO <sub>3</sub> /5.4                            |
| 6               | SnO <sub>2</sub> nanopowder                  | <100 nm               | Sigma-Aldrich                    | 8 $\mu\text{m}$                   | 3.65                              | MgO/6.40  |
| 7               | SnO <sub>2</sub> nanotube                    | 110 nm                | electrospinning                  | 13 $\mu\text{m}$                  | 0.99                              | TiCl <sub>4</sub> /5.11                           |
| 8               | SnO <sub>2</sub> hollow nanospheres          | 200 nm                | hydrothermal                     | ---                               | 0.86                              | TiCl <sub>4</sub> /6.02                           |
| 9               | SnO <sub>2</sub> octahedra                   | 0.5-1.8 $\mu\text{m}$ | sonochemical                     | 13.2 $\mu\text{m}$                | ---                               | TiCl <sub>4</sub> /6.8                            |
| 10              | mesoporous SnO <sub>2</sub> agglomerates     | 200-600 nm            | molten salt method               | 8 $\mu\text{m}$                   | 3.05                              | TiCl <sub>4</sub> /6.23                           |
| 11              | SnO <sub>2</sub> nanofibers                  | 200 nm                | ---                              | 8.7 $\mu\text{m}$                 | --                                | TiCl <sub>4</sub> /4.63                           |
| <b>Our work</b> | <b>Ga-SnO<sub>2</sub>hollow microspheres</b> | <b>11.6-15.9 nm</b>   | <b>hydrothermal</b>              | <b>8 <math>\mu\text{m}</math></b> | <b>3.56</b>                       | <b>TiCl<sub>4</sub>/7.11</b>                      |

<sup>a</sup>surface treatment method and the corresponding photon-to-electron conversion efficiency.

**Table S2.** Calculated structural parameters a and c for pure SnO<sub>2</sub> and 6.25% Ga doped SnO<sub>2</sub>.

| Experiment for SnO <sub>2</sub> | Calculation for SnO <sub>2</sub> | Calculation for Sn <sub>0.9375</sub> Ga <sub>0.0625</sub> O <sub>2</sub> | Calculation for 6.25% Ga interstitial doping |
|---------------------------------|----------------------------------|--|--|
| a (Å)                           | 4.74 <sup>b</sup>                | 4.76   | 4.75   |
| c (Å)                           | 3.19 <sup>b</sup>                | 3.21   | 3.20   |

<sup>b</sup>Phys. Rev. B. 81, 245216, 2010

## References

1. M. K. I. Senevirathna, P. Pitigala, E. V. A. Premalal, K. Tennakone, G. R. A. Kumara and A. Konno, *Sol. Energy Mater. Sol. C*, 2007, **91**, 544-547.
2. S. Gubbala, V. Chakrapani, V. Kumar and M. K. Sunkara, *Adv. Funct. Mater.*, 2008, **18**, 2411-2418.
3. J. F. Qian, P. Liu, Y. Xiao, Y. Jiang, Y. L. Cao, X. P. Ai and H. X. Yang, *Adv. Mater.*, 2009, **21**, 3663.
4. X. C. Dou, D. Sabba, N. Mathews, L. H. Wong, Y. M. Lam and S. Mhaisalkar, *Chem. Mater.*, 2011, **23**, 3938-3945.
5. K. Perera, S. G. Anuradha, G. R. A. Kumara, M. L. Paranawitharana, R. M. G. Rajapakse and H. M. N. Bandara, *Electrochim. Acta*, 2011, **56**, 4135-4138.
6. P. Docampo, P. Tiwana, N. Sakai, H. Miura, L. Herz, T. Murakami and H. J. Snaith, *J. Phys. Chem. C*, 2012, **116**, 22840-22846.
7. C. T. Gao, X. D. Li, B. G. Lu, L. L. Chen, Y. Q. Wang, F. Teng, J. T. Wang, Z. X. Zhang, X. J. Pan and E. Q. Xie, *Nanoscale*, 2012, **4**, 3475-3481.
8. H. Wang, B. Li, J. Gao, M. Tang, H. B. Feng, J. H. Li and L. Guo, *Crystengcomm*, 2012, **14**, 5177-5181.
9. Y. F. Wang, K. N. Li, C. L. Liang, Y. F. Hou, C. Y. Su and D. B. Kuang, *J. Mater. Chem.*, 2012, **22**, 21495-21501.
10. P. N. Zhu, M. V. Reddy, Y. Z. Wu, S. J. Peng, S. Y. Yang, A. S. Nair, K. P. Loh, B. V. R. Chowdari and S. Ramakrishna, *Chem. Commun.*, 2012, **48**, 10865-10867.
11. R. Kasaudhan, H. Elbohy, S. Sigdel, Q. Hui, W. Qufu and Q. Qiquan, *Electron. Device Lett., IEEE* 2014, **35**, 578-580.